T cell/Macrophage Dual-Targeting Biomimetic Triptolide Self-Assembly Nanodrugs For Rheumatoid Arthritis Therapy by Inflammatory Microenvironment Remodeling

Jing Li[1], Sanpeng Li[1], Chunbin Li[1], Hongfeng Li[1], Chuangjun Liu[1], Qi Zhao[3], Pengfei Zhang[1], Ping Gong[1,2*], Lintao Cai[1*]*

1Guangdong Key Laboratory of Nanomedicine, CAS-HK Joint Lab for Biomaterials, Shenzhen Institutes of Advanced Technology, Chinese Academy of Sciences, Shenzhen 518055, China

2Guangdong Key Laboratory for Research and Development of Natural Drugs, Guangdong Medical University, Dongguan, 523808, China

3 Faculty of Health Sciences, University of Macau, Taipa, Macau, China.

* E-mail addresses: pf.zhang@siat.ac.cn, ping.gong@siat.ac.cn, lt.cai@siat.ac.cn.

ABSTRACT

Rheumatoid arthritis (RA) is an autoimmune disease causing severe joint damage, disability and decreased quality of life. Pathologically, numerous blood-derived cells infiltrating in synovium and cytokine secret necessitating formation of new blood vessels to generate pannus together form an inflammatory microenvironment. Triptolide with immunosuppressive activities is a potential drug to treat RA. However, it is still lack of an effective targeting system to deliver triptolide to RA site safely. Herein an inflammatory microenvironment targeting and remodeling nanoplatform is developed to achieve significantly effective RA treatment. In this system we synthesized a self-assembling triptolide nanoparticles (TPNs) mediated by dipeptide diphenylalanine which is the simplest self-assembly building block, then TPNs were entrapped by mannose-modified erythrocyte membranes to form engineering manRTPNs. For targeting, the immunological molecule of erythrocytes was firstly introduced to target T cells by ligand-binding of LFA-3/LFA-2, and the coated mannose modified erythrocyte membrane also conferred the capacity of targeting to macrophages by mannose and its receptor CD206; for remodeling inflammatory microenvironment, TPNs could selectively exert its suppressive effects on different cells of RA including lymphocytes and synovial fibroblasts. In collagen-induced arthritis mice, manRTPNs showed excellent targeting effect and prolonged accumulation at inflamed joint. After manRTPNs treatment, swollen paws of CIA considerably shrunk to normal, boss loss even recovered healthy level and cartilage preserved at synovium cavity, because of systemically conventional cytokine reduction and expression shift of core genes in networks

of RA microenvironment. Therefore, this well-defined manRTPNs might be a well promising systematic therapeutic agent for RA.

KEYWORDS : Triptolide, Peptide self-assembly, Nanodrug, Inflammatory microenvironment

, Rheumatoid arthritis.

Rheumatoid arthritis (RA) is a serious long-term disease characterized by persistent synovitis, systemic inflammation and autoantibodies and causing severe joint damage, disability and decreased quality of life. Its etiopathogenesis remains elusive; treatment options are limited, and outcomes are mostly poor.[1, 2] Over the last two decades, long-term management of RA has involved disease-modifying anti-rheumatic drugs (DMARDs), biological agents such as tumor necrosis factor (TNF) inhibitors, and glucocorticoids.[3] Although the highest clinical remission rate achieved within 50% of control, not all patients attain desirable levels of clinical remission[4] and clinical use of these therapies is limited because of their high cost and the frequency of adverse effects. The latter includes teratogenicity and hepatotoxicity of DMARDs like methotrexate,[5, 6] risks of infections such as tuberculosis and osteoporosis caused by biological agents[7, 8] and long-term glucocorticoids.[9, 10] In RA pathogenesis, numerous blood-derived cells infiltrating in synovium, numerous pro-inflammatory cytokines secreting, angiogenesis to generate pannus, a progressive destruction of cartilage and bone, that all of these forms an inflammatory microenvironment.[11] Lately,

new therapies aim to inflammatory factors such as neutrophils,[12] macrophages[13] and cell-free DNA (cfDNA)[14] in inflamed joint or some based methotrexate delivery system[15] have been reported, but inhibiting a single factor may not be enough to sustainably halt or reverse disease progression due to RA's complexity and heterogeneity. Therefore, a new strategy simultaneously inhibiting multi-factors in inflammatory microenvironment is highly desirable for efficient rheumatoid arthritis therapy.

Triptolide is a complex natural triepoxide diterpene product of *Tripterygium wilfordii* (or *Léi Gōng Téng*), an herb used in traditional Chinese medicine; Chinese *Léi Gōng Téng* multiglycoside tablets have been available for RA treatment since the 1970s, and triptolide is regarded as main bioactive ingredients of it.[16] Despite triptolide's various biological activities like immunosuppressive effect, poor water solubility, severe multi-organ toxicity especially to the liver and kidney, and narrow therapeutic window remain an unresolved barrier to clinical applications of it.[17] Several triptolide analogs have been developed and evaluated, mainly including (5R)-5-hydroxytriptolide (LLDT-8)[18], PG490-88[19] and glucose[20] or aptamer[21] conjugation. These derivatives increase water solubility or decrease the toxicity, while direct conjugations attached to the C_{14}-hydroxyl group of triptolide via a hydrolytic ester bond have proven biologically unstable and these structures haven't further produced nanoparticles. Current targeted delivery systems for triptolide have limited drug loading or encapsulation ratios and are mostly targeted at the kidney or tumors, like nanoformulations coated with folate,[22] pH-sensitive nanoformulated triptolide.[23] In contrast, the nanoformulation of chemical drugs seemed to be one promising approach for increasing the drug content but

reducing the side effect. Therefore, an effective and stable deliver system for triptolide is highly desirable.

On the other side, drug-induced nanoparticles have own advantage including changing pharmacokinetics and toxicity profiles of parental drugs, specific accumulation in the specific site and releasing drugs at a synchronized rate.[24] However, direct conjugating with glucose, triptolide hasn't assembled into nanoparticles.[20] Inspired from biomacromolecule self-assembly process, various peptide building blocks have been performed for the creation of biomimetic or bioinspired nanostructured materials.[25, 26] Recently, diphenylalanine (Phe-Phe, FF) is the simplest peptide building block for self-assembly and exhibits remarkable advantages including biocompatibility and non-immunogenicity and so on. Many researchers have developed Phe-Phe-based nanomaterials such as nanotubes, spherical vesicles, nanofibrils and nanowires.[27] However, it is barely to link diphenylalanine with parent drugs for nanoparticles formation. Therefore, peptide based self-assembly nanoparticles may be an advance for triptolide further application.[28]

Macrophages are central effectors of synovial inflammation in RA and their abundance and degree of activation are correlated with disease severity.[29] In RA, precursors from the monocyte/macrophage lineage are attracted from the blood to the inflamed joint and functionally diverse macrophages distribute in the synovial sublining and lining layers.[30] Besides, T cells represent approximately 40% of immune cells in the synovial infiltrate of RA joints. In RA pathology, activated T cells produce cytokines and induce cytokine production by other cells, and also promote development of an autoimmune response and production of

autoantibodies.[31, 32] Synovial fibroblasts (FLSs) release matrix-degrading enzymes, including matrix metalloproteinases (MMPs) and cathepsins, which cause cartilage destruction.[33] Therefore, macrophage and T cell are potential targeting cells guiding to pathogenesis of arthritis.[34] Furthermore, it is mentioned that Cluster of Differentiation 206 (CD206) on macrophages surface has been induced to express more.[29] Certain signal proteins on the T cell surface such as lymphocyte function antigen 2 (LFA-2) also have increased in both RA patients and animal models.[35, 36] Interestingly, LFA-3, the ligand of LAF-2 widely distributes on erythrocyte membranes and LFA-3/LFA-2 interaction has mediated process of T cells activation. Meanwhile, LFA-2 can be effectively targeted by peptides derived from LFA-3 and its fusion protein constructs.[37] This immunological characteristic of erythrocytes scarcely ever attracts attention in application, so it is a valuable attempt to apply in drug targeting. Then, mannose, the ligand of CD206 could be introduced in erythrocyte membrane for macrophage targeting.[38] In addition, the long circulation and flexible functionalization of erythrocyte membrane also make it be a promising platform and have wide application.[39]

In this work, we have developed nanoconstructed an effective nanomedicine system targeting to inflammatory microenvironment of joints and maximizing utility of triptolide (**Figure 1A**). A small molecular amphiphile (Triptolide-Phe-Phe-Glucose, TP-FF-AG, MW ~ 874) for self-assembling of triptolide nanodrugs was synthesized. Self-assembling triptolide nanoparticles (TPNs) have obtained a successful structural modification for original drug and make it less toxicity and more structural stability than reported cases. The coated mannose modified erythrocyte membrane conferred the capacity of targeting to inflamed cells for

manRTPNs mediated by two ligand-receptor pairs of mannoses and CD206, LFA-3 and LFA-2. According to manRTPNs, its multiple effects weren't just specifically inducing cell death in inflamed joints, but remodeling the inflammatory microenvironment through affecting genes network, downregulating cytokines and pro-angiogenic factors, and regulating balance of metalloproteinases (MMPs) and their inhibitors (TIMPs). Therefore, this triptolide nanodrugs showed high drug content, low side effect, good biocompatibility which showed great potential for clinical rheumatoid arthritis therapy.

RESULTS AND DISCCUSION

Triptolide modification and manRTPN nanoparticles preparation

Triptolide is a diterpene triepoxide with several active sites that can be modified, especially C_{14} position.[40] Because of its hydrophobicity, triptolide molecule acted as self-assembly inducer with the addition of diphenylalanine peptide (FF), which is the key moiety of the self-assembling peptide-drug conjugate. Initially, we added a glucosamine (AG) to the FF terminal to lengthen the hydrophilic chain, and then linked triptolide to FF-AG by an ester bond whose cleavage led to drug release in the cell; thus, the self-assembling monomer (TP-FF-AG) as a triptolide prodrug was synthesized. We confirmed the chemical structures of these compounds via mass spectrometry (MS) and nuclear magnetic resonance (NMR; **Figure S2-S17**). Due to hydrophobic interactions, triptolide nanoparticles (TPNs) were formed via self-assembly of synthesized monomer namely TP-FF-AG, which is uniformly easy to control TPNs size in water solution. We confirmed the particles morphology via transmission electron microscopy (TEM; **Figure 1b**). To synthesize manRTPNs, we coated

mannose-modified erythrocyte membranes onto TPNs using an extruder to form a core-shell structure (**Figure 1b**). Dynamic light scattering (DLS) measurements revealed that the TPNs were 135 nm in hydrodynamic diameter and manRTPNs were about 10 nm larger with PDIs of 0.15-0.2. The surface zeta potential of the shell was not as negative as that of the cores but was comparable to that of erythrocyte membrane-derived vesicles (RBC vesicles) (**Figure 1c**). All these results demonstrated successful cloaking of TPNs with erythrocyte membranes.

Next, TPNs and manRTPNs were stored in phosphate-buffered saline (PBS) for 1 month, where they demonstrated a negligible change in size and showed an excellent stability (**Figure 1d**). Maintaining protein compounds of erythrocyte membranes on nanoparticles' surfaces is vital for harnessing their biofunctionality. Therefore, we verified the completeness of the membrane coating via sodium dodecyl sulfate polyacrylamide gel electrophoresis (SDS-PAGE; **Figure S18**), which indicated the manRTPNs maintained the whole effective biocomponent of erythrocyte on the surface. Translocation of erythrocyte membranes might improve the biocompatibility and circulating period of TPNs in vivo, which also sustains systemic delivery and better targeting through both passive and active uptakes.[41] As reported, the elimination $T_{1/2}$ of triptolide molecules in rats following *i.v.* administration was 15-21 minutes, which showed that drugs were rapidly eliminated.[42] However, TPNs and manRTPNs have maintained higher plasma concentration after tail intravenous injection of mice in our work. As the relative signal of drug down to 50%, TPNs lasted 4 h, and manRTPNs even had a much longer elimination half-life of over 48 hrs (**Figure 1e**), which suggested that manRTPNs significantly expanded blood circle compared to triptolide. Therefore, the self-

assembling TPNs nanostructure was more stable than original drug, and manRTPNs inherited erythrocyte membrane proteins to have bioability for following efficacy.

Targeting capacity and efficacy of manRTPNs in inflammatory cells

The main mechanism by which manRTPNs target to activated macrophages and T cells in inflamed joints is the ligand-binding of mannose/CD206 and LFA-3/LFA-2, respectively. To determine the targeting capacity of manRTPNs to inflamed cells in vitro, nanoparticles were Cy5.5-labelled and incubated with macrophages and T cells activated with IL-4 (100 ng/mL) or TNF-α (10 ng/mL), untreated cells as control. Flow cytometry (FCM) analysis observed gradual increased uptake of nanoparticles by macrophages and T cells for 6 hrs (**Figure S19-21**). An uptake curve was built using mean fluorescence intensity (MFI) of cells at six time points, and cellular uptake rate was defined as *k* indicated in **figure 2a-c**, which was the slope of the uptake curve. In detail, *k*s of nanoparticles in treated macrophages and T cells were significantly higher than that in untreated cells (**Figure 2a-c**; **Figure S22A**), and *k*s of manRTPNs were significantly higher than that to TPNs both in macrophages and T cells (**Figure 2a-b**), but no difference of *k*s existed between TPNs and manRTPNs in fibroblasts-like synoviocytes which was no targeting ligands on it (**Figure 2c**), which was attributed to the increased expression of surface molecules and stronger ligands interactions between manRTPNs and macrophages or T cells. Further, the k value in macrophages was higher than that in T cells (**Figure 2a-b**), indicating macrophages existed effective phagocytosis. To further confirm the ligand-binding specificity, Cy5.5-labelled TPNs (without mannose and LFA-3), RTPNs (with LFA-3) and manRTPNs (with mannose and LFA-3) were incubated

with treated macrophages and T cells for 3 hrs as well, FLSs and hFLS-RA as control. After treatment, CLSM images showed that CD206 and LFA-2 (**Figure 2d-e**, green) respectively overexpressed on surface of macrophages and T cells. Significant red fluorescence was observed on macrophages incubated with manRTPNs, but not with TPNs and RTPNs (**Figure 2d**), while red fluorescence was observed on T cells incubated with RTPNs and manRTPNs but not with TPNs (**Figure 2e**), which was consistent with corresponding ligands distribution on the nanoparticles. When co-incubated with FLSs, they also entered cells (**Figure 2f**; **Figure S22b**). Similar results were observed in flow cytometry analysis (**Figure 2g-i**; **Figure S22c**). These results demonstrated the ability of manRTPNs to target inflamed cells conferred by their mannose modified erythrocyte membrane coating. The binding is probably attributed to specific interactions between mannose and LFA-3 on the erythrocyte membranes and CD206 and LFA-2 overexpressed on activated macrophages and T cells.

To determine efficacy of manRTPNs in joint inflammatory microenvironment, three kinds representative and proliferative cells including activated macrophages, T cells, FLSs and hFLS-RA were incubated with manRTPNs in 96-well plates for 24 hrs, untreated cells as control. Firstly, cell viability was measured via MTT assay. TPNs and manRTPNs didn't significantly reduce macrophages viability even at a concentration of 500 nM (**Figure 3a**). However, at the same concentration T cells, FLSs and hFLS-RA showed an obvious cytotoxicity (**Figure 3b-d**). Specially, manRTPNs had an IC_{50} (half maximal inhibitory concentration) values of 219 nM for T cells cytoxicity, 88.9 nM for rat FLSs cytoxicity and 95.8 nM for human FLS-RA (hFLS-RA) cytoxicity (**Figure 3b-d**). The lower IC50 values of

activated FLSs and hFLS-RA indicated that triptolide-induced cell death was mainly against anomalous proliferative synoviocytes in inflamed joints, rather than lymphocytes like macrophages. In the progress of RA pathology, many inflammation molecules produced by cells have already been elevated. To determine corresponding efficacy of manRTPNs on inflamed cells, cells were following collected and lysed for mRNA extraction to check certain genes variation by qPCR. For macrophages, transcription factor *NF-κB* associated with most cytokine transcription[43] and *cyclooxygenase-2* (*cox-2*) were induced to decrease expression level, but *tissue inhibitor of metalloproteinase-1* (*timp-1*) showed opposite variation under manRTPNs treatment. *Receptor activator of NF-κB ligand* (*rankl*) over-expressed on T cell was also downregulated by manRTPNs. Vascular endothelial growth factor (VEGF) being critical for angiogenesis and metalloproteases including MMP-2 and MMP-9 degrading cartilage extracellular matrix (ECM) overexpressed by FLSs in RA responded manRTPNs to lessen their gene transcripts (**Figure 3e**). Thirdly, medium supernatants were collected to measured cytokines by ELISA assay. supernatant IL-1β and IL-6 of macrophages and supernatant IFN-γ of T cells lessened more quickly that treated with manRTPNs than TPNs (**Figure 3f-h**), while supernatant IL-1β and IL-6 of rat FLSs had a similar decreasing curve between TPNs and manRTPNs groups (**Figure 3i-j**), which indicated that manRTPNs had superior identification of immune cells than resident synoviocytes at least in cytokine secretion. Consequently, manRTPNs could regulate genes and proteins expression involved in pathways associated inflammation for certain cell. These results showed that manRTPNs selectively exerts its suppressive effects on different cells in RA. It couldn’t only induce

lymphocytes and synovial fibroblasts cell death, but also regulate production of proinflammatory cytokines, proinflammatory mediators and matrix metalloproteinases, which suggested manRTPNs may have an ability to remodel inflammatory microenvironment through its cell-specific efficacy.

Targeting to inflamed joint and accumulation in CIA mice of manRTPNs

Upon the good capacity of manRTPNs to target activated macrophages and T cells in vitro, we further verified their ability to target RA site in vivo. After CIA mouse model being induced, all four paws swelled in varying degrees.[44] Hind paws were more heavily swollen, and micro-computed tomography (Micro-CT) imaging showed distinct bone loss of joint therein (**Figure 4a**). Then these mice received intravenous injections of free cyanine 5.5 (Cy5.5) solution and Cy5.5-labelled TPNs and manRTPNs for targeting imaging in vivo. As shown in **Figure 4a**, almost no fluorescence signal was detected in paws of the free-Cy5.5 group, indicating that the dye barely accumulated at local inflammatory sites. In the TPNs group, we detected a weak signal, which peaked after 4 h (**Figure 4a**). While manRTPNs obviously reached the RA sites and lasted there for ≥12 hrs, which would be attributed to their long circulation and the targeting effect of the modified erythrocyte membranes. Thus, significant fluorescence of manRTPNs lasted longer and showed greater accumulation than that of TPNs. 24 hrs after intravenous injections, we dissected mouse and got froze sections of left paws to observe nanoparticles' retention in the inflamed joints. Contrary to free-Cy5.5 and TPNs group, fluorescence microscopy indicated a very high fluorescence intensity of manRTPNs in the synovial sublining layer, resulting in a reduced accumulation at the

inflamed joint due to the lack of permeability (**Figure 4b**). Tissue biodistribution further revealed manRTPNs' outstanding capacity to target the paws of RA mice, rather than other groups (**Figure 4c**). Additionally, higher accumulation was observed in liver, suggesting that this organ might be passive targeting of nanoparticles and the main organ metabolizing triptolide (**Figure 4c**). The results confirmed that the effective accumulation of manRTPNs provided a promising precondition of RA treatment.

Therapeutic efficacies and shifting inflammatory factor of manRTPNs in CIA mice

Since precise targeting of manRTPNs and sufficient drug accumulation at inflamed joints, we evaluated its efficacy of ameliorating joint damage in the CIA mouse model. Following arthritis induction, CIA mice presented symptoms of swelling in ankle and paw joints and a clinical scoring was used to estimate the swelling degree (**Figure S24**). According to protocol timeline, CIA mice were treated with intravenous injections of triptolide, TPNs and manRTPNs at doses of 25 mg/kg for 11 days, healthy mice, and PBS, RBC vesicles treated mice as positive and negative controls (**Figure 5a**). Surprisingly, the swollen hindpaws and forepaws both shrunk considerably and even recovered to the same extent as healthy ones with manRTPNs treatment rather than slightly shrunk in TPNs and triptolide group, but swelling symptoms in other groups were more and more severe (**Figure 5b**), implying that inflammation process was exactly controlled by manRTPNs. As paw swelling is only a surface phenomenon of RA, bone loss was further determined using Micro-CT analysis. Micro-CT analysis reconstructed three dimensional (3D) bones images and calculated bone mean density (BMD). These results showed that serious bone erosion appeared in paw joints

in all model mice except for healthy mice before treatment (**Figure 5c-d**). After treatment, 3D images presented that bone morphology of manRTPNs group had recovered to healthy mice, and the BMD variation also rose to healthy levels (**Figure 5c-d**), suggesting a protective role of manRTPNs on preserved trabecular bone despite joint inflammation. Then, ankle joints of the mice were further sectioned for histological analysis. Haemotoxylin and eosin (H&E)-stained sections from the manRTPNs group showed the reduction of immune infiltration and preservation of cartilage at the synovium and articular cavity. In contrast, an intense anomalous proliferative cells infiltration in the joints and synovium were observable in control groups (**Figure 5e**). Therefore, these results illustrated remarkable therapeutic effect of manRTPNs against RA.

To elicit a systemic therapeutic response of manRTPNs, mechanism was investigated through cytokines expression including TNF-α and IL-6, which are known to increase with the onset of arthritis and correlate strongly with disease severity.[45] Immunohistochemical analysis showed that TNF-α and IL-6 of synovium and articular cavity significantly declined in triptolide, TPNs and manRTPNs groups (**Figure 6a-b**) and serum levels of TNF-α and IL-6 also observed to alleviate similarly (**Figure 6c**), indicating effective reduction of arthritis at cytokines level. Heatmap of genes expression in CIA mice showed that manRTPNs suppressed several genes expression including *rank*, *rankl*, *vegf*, *vegfr2*, *NF-κB*, *cox-2*, *IL-1β*, *mmp-2*, *mmp-3*, *mmp-9* and *mmp-13* that amounts of these transcripts were dramatically increased in the joints of the CIA mice and augmented mRNA of *opg*, *timp1* and *timp2* (**Figure 6d**), indicating manRTPNs simultaneously regulated production and gene expression

of mediators constituting inflammatory microenvironment in RA process. Actually, the bone destruction occurred in RA is regulated by the receptor activator of nuclear factor-κB (RANK) ligand (RANKL), and RANKL/RANK/OPG signal pathway was regulated by manRTPNs in the process of bone destruction (**Figure 6e**), because of balance of RANKL and its receptor RANK inducing osteoclast-mediated bone destruction, and OPG inhibition.[46] manRTPNs also ameliorated extracellular matrix (ECM) and basement membrane destroying and pannus formation through regulated the balance of metalloproteinases and their inhibitors (TIMP) and pro-angiogenic factors VEGF and its receptor 2 (VEGFR2) (**Figure 6e**)). In brief, manRTPNs remodeled the RA inflammation microenvironment in various and multiple ways, thus it was an effective and systematic agent to ameliorate inflammatory joints.

Biosafety of manRTPNs nanoparticles

To investigate safety and biocompatibility of TPNs and manRTPNs in vivo, we administered PBS, TPNs or manRTPNs at a single dose of 25 mg/kg to healthy mice via tail vein, while to other mice we administered triptolide (original drug of TPNs and manRTPNs) at 15 mg/kg by intraperitoneal injection. It is worth mentioning that most mice in the triptolide group died soon (within 24 hrs) after 25 mg/kg administration, indicating the high toxicity of the original drug (**Figure S25**). After 1-week treatment, mice treated with triptolide showed a significant decrease in count of white blood cells (WBC), RBCs and platelets (**Figure 7a**), suggesting the occurrence of bone marrow suppression, which is one of the main side effects of triptolide. The main three type cells comprised WBC including neutrophils, lymphocytes, and monocytes showed significant count differences between

triptolide group and other groups, which explained the WBC count variation conferred from triptolide (**Figure 7b**). The hemoglobin concentration did not differ significantly among all the groups in the blood (HGB), mean corpuscular hemoglobin (MCHC) level, and hemoglobin distribution width (HDW) (**Figure 7c**), indicating that triptolide didn't influence the physiological function of RBCs. Blood biochemistry analysis showed that blood urea nitrogen (BUN), aspartate aminotransferase (AST), creatinine (Cr) and lactate dehydrogenase (LDH) levels of mice treated with triptolide were significantly higher than those of mice in the TPNs and manRTPNs groups (**Figure 7d-g**). These variations demonstrated that the hepatotoxicity and nephrotoxicity of triptolide were greatly reduced in TPNs, with RBC membrane coating yielding even better safety. Hematoxylin and eosin (H&E) staining of major organs showed that triptolide treatment caused inflammatory infiltration of the liver and severe renal injury characterized by loss of the brush border, tubular epithelial cells detachment from the basement membrane and tubular obstruction. Meanwhile, the TPNs and manRTPNs groups showed no significant variation in cellular morphology and negligible organ damage, in line with the PBS group (**Figure 7h**). However, TPNs and manRTPNs significant reduced triptolide toxicity.

Conclusion

Natural products continue to serve as important and invaluable sources of new-drug discoveries. Triptolide is a representative natural product with multiple biological activities and has huge potential to develop new drugs aim at cancer and autoimmune diseases. Through connecting with dipeptide, triptolide itself being the inducer has performed to

engineer toxic drug nanoformulation solving the problems of drug loading, toxicity and poor water solubility. Meanwhile, immunological characteristic of erythrocytes was firstly applied in drug targeting, which was a valuable attempt to deep into red blood cell. Therefore, this combined system had selectively exerted its suppressive effects on gene and protein networks of different cells, which couldn't only induce lymphocytes and synovial fibroblasts cell death, but also regulate production of proinflammatory cytokines, proinflammatory mediators and matrix metalloproteinases. In addition, manRTPNs have kept multiple biological activities of triptolide, and been on good behavior of suppressing the inflammatory responses and cartilage destruction in the CIA model. On deep level, complexity and specificity of triptolide make it be a multifunctional drug and clearly distinguish it from other agent such as dexamethasone. It should be pointed out that triptolide nanodrug have selectively exerted its suppressive effects on different cells, regulated production of proinflammatory cytokines like IL-6 and TNF-α and genes expression of proinflammatory mediators such as NF-κB, cox-2. Triptolide and its nanodrug are on good behavior of suppressing the inflammatory responses. Therefore, triptolide or triptolide-based nanodrugs could be potentially used as a candidate drug to inhibit the inflammatory storm caused by viral infection (such as H5N1, H1N1, SARS-CoV-2, etc).

FIGURES

Figure 1. Preparation and Characterization of manRTPNs.

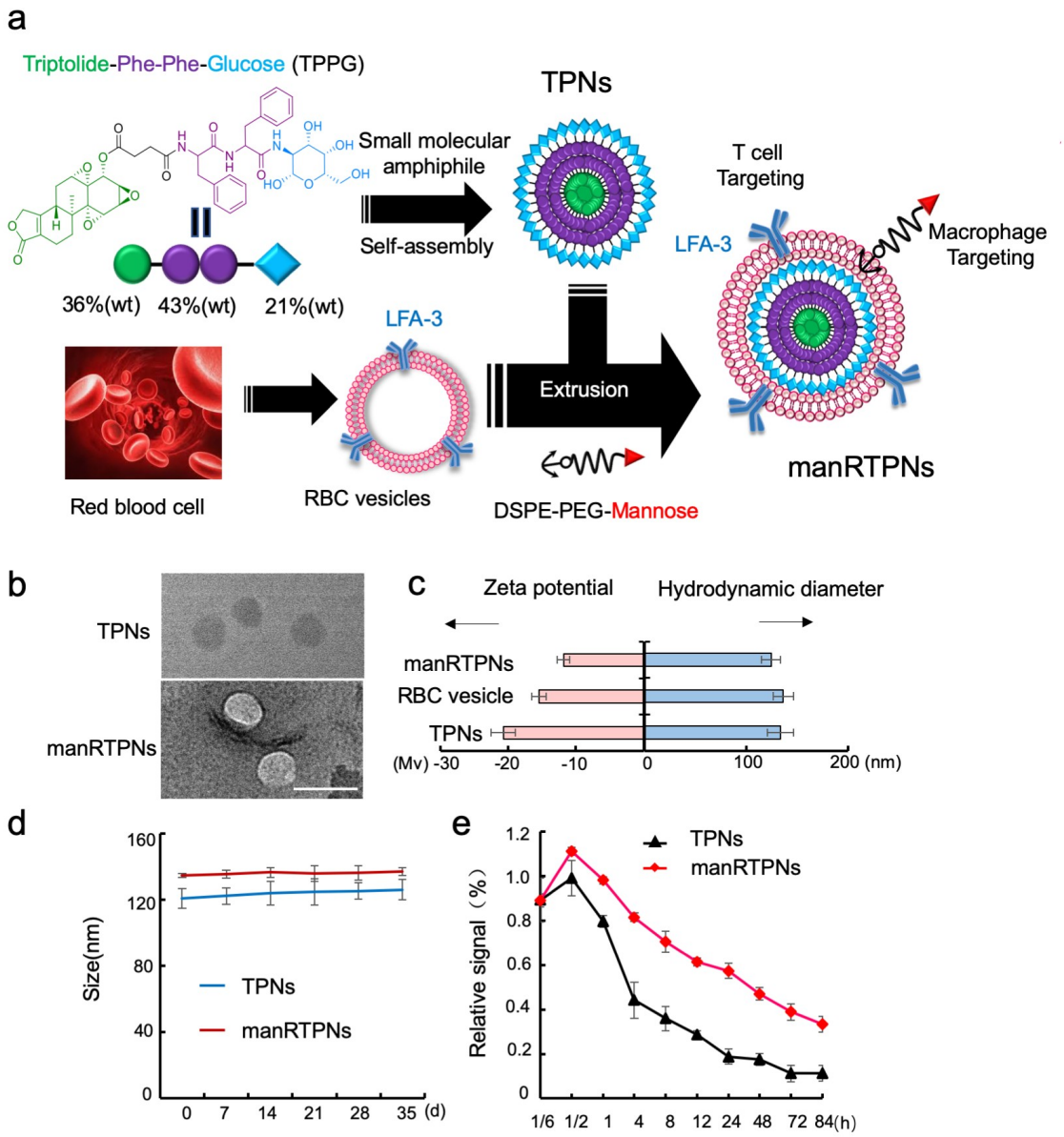

(a) Schematic illustration of erythrocyte membranes-coating triptolide self-assembling nanoparticles (manRTPNs). (b) Representative image of TPNs and manRTPNs examined with transmission electron microscopy (TEM). manRTPNs samples were stained with uranyl acetate. Scale bar, 200 nm. (c) Size and ζ potential distribution of TPNs, RBC vesicles and manRTPNs. Each experiment had three replicates. (d) Stability of TPNs and manRTPNs in PBS over five weeks. Each experiment had three replicates. (e) Pharmacokinetics of TPNs and manRTPNs in vivo. Each experiment point had three replicates.

Figure 2. Targeting capacity to immune cells of manRTPNs.

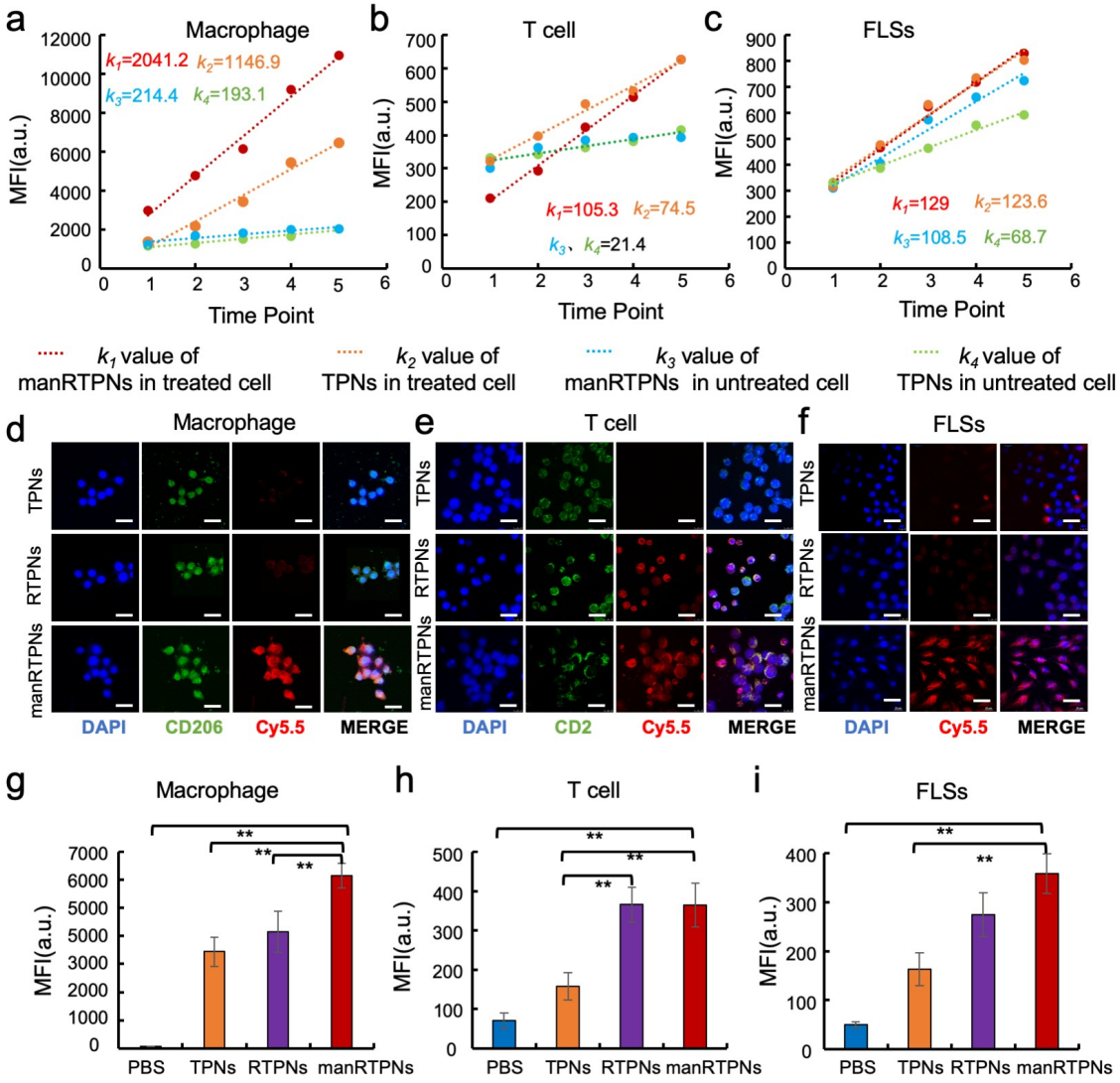

(a-c) Cellular uptake capacity of TPNs and manRTPNs in three cell lines. Flow cytometry analysis of TPNs and manRTPNs were conducted in RAW246.7 (a), CTLL-2 (b) and RSC364 (c). k was slope of uptake curve built with mean fluorescence intensity (MFI) which indicated cell uptake rate. (d-f) Representative fluorescence images by confocal analysis. RAW246.7 (d), CTLL-2 (e), and RSC364 (f) were co-incubated with TPNs, RTPNs (e), and manRTPNs (f), respectively. Nanoparticles were labeled with Cy5.5 (red), CD206/LFA-2 antibody (green) expressed on the IL-4 -treated macrophages and TNF-α treated T cells and

cellular nuclear was labeled with DAPI (blue). Scale bars, 100 μm. (g-i) Flow cytometry analysis of RAW246.7 (g), CTLL-2 (h) and RSC364 (i) incubated with various nanoparticles. ** indicated significant difference and $p < 0.05$.

Figure 3. Efficacy of manRTPNs in inflammatory cells.

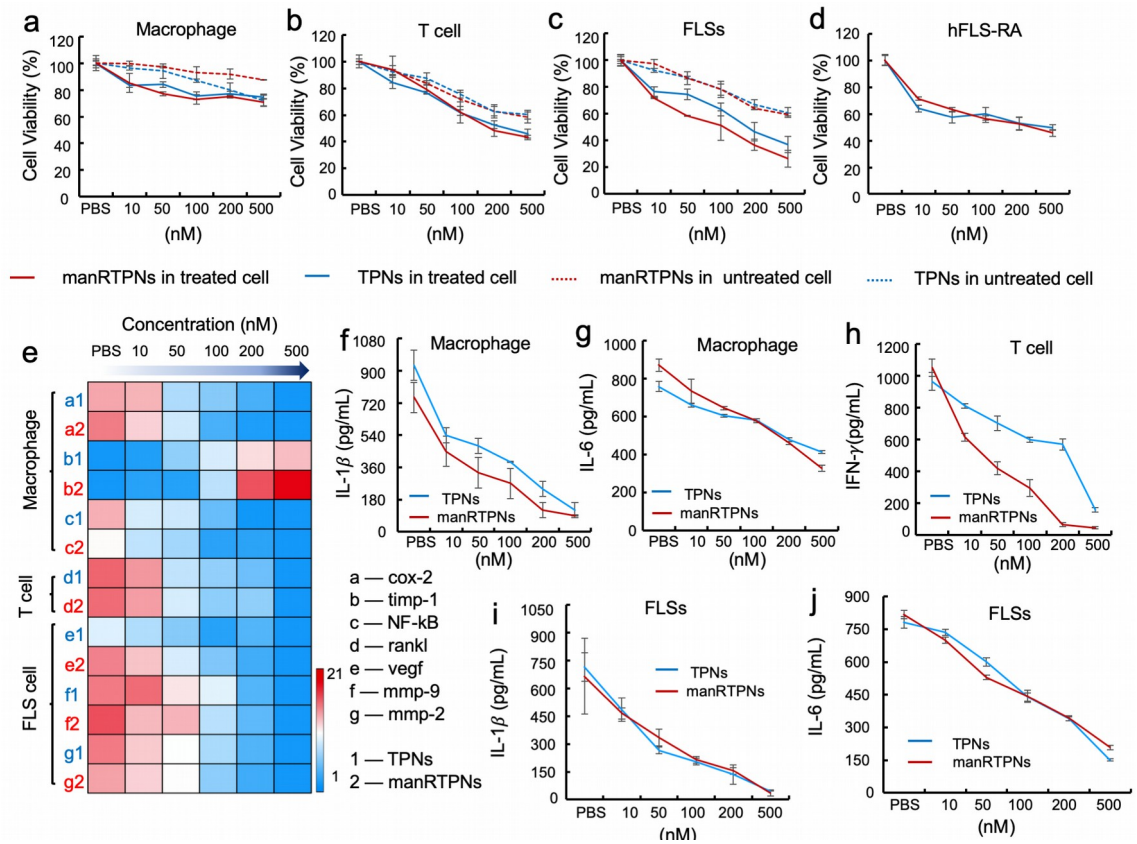

(a-d) Cytotoxicity of TPNs and manRTPNs in RAW264.7 (a), CTLL-2 (b), RSC364 (c), and hFLS-RA (d). Each experiment point had three replicates. (e) Heatmap of inflammatory factors genes expression. Briefly, genes cox-2, timp-1 and NF-κB were checked in RAW264.7, gene rankl was checked in CTLL-2 and genes vegf, mmp-9 and mmp-2 were checked in RSC364, respectively. (f-j) Cytokines concentration variation of inflammatory cells treated with TPNs and manRTPNs. Supernatant IL-1β was measured in RWA264.7 (f)

and RSC364 (i), supernatant IL-6 in RWA264.7 (g) and RSC364 (j), supernatant IFN-γ in CTLL-2 (h), each experiment had three replicates.

Figure 4. Targeting effect and accumulation at inflamed site of RA of manRTPNs.

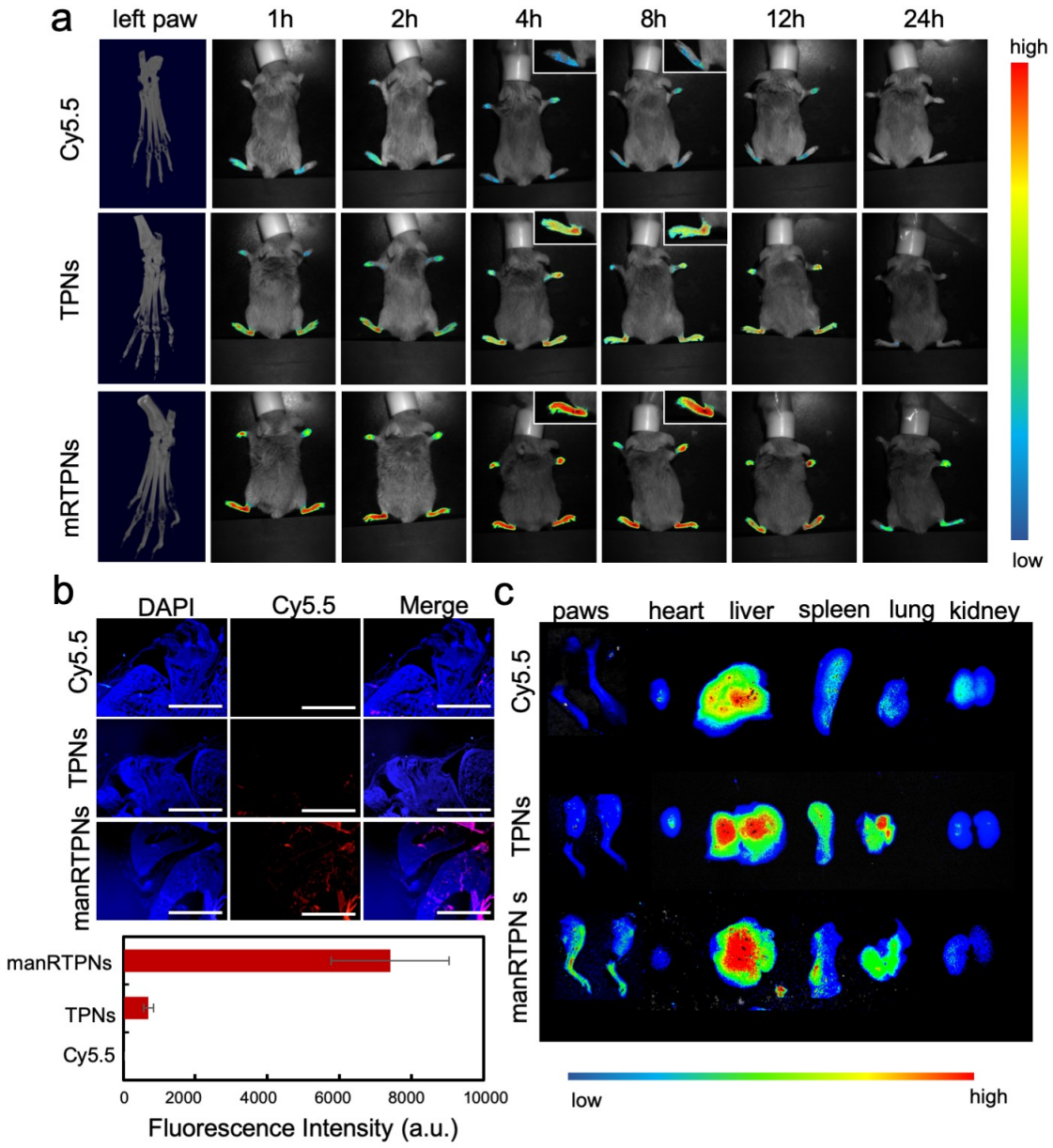

(a) Representative images of free Cy5.5, TPNs and manRTPNs accumulating in arthritic paws. (b) Fluorescence images of free Cy5.5, TPNs and manRTPNs in arthritic paws fixed after 24 hours of intravenous injection. Scale bars, 500 μm. Fluorescence of free Cy5.5, TPNs

and manRTPNs was quantified in arthritic paws sections. (c) Distribution of free Cy5.5, TPNs and manRTPNs in main organs and arthritic paws.

Figure 5. Therapeutic effect of manRTPNs in a mouse model of collagen-induced arthritis.

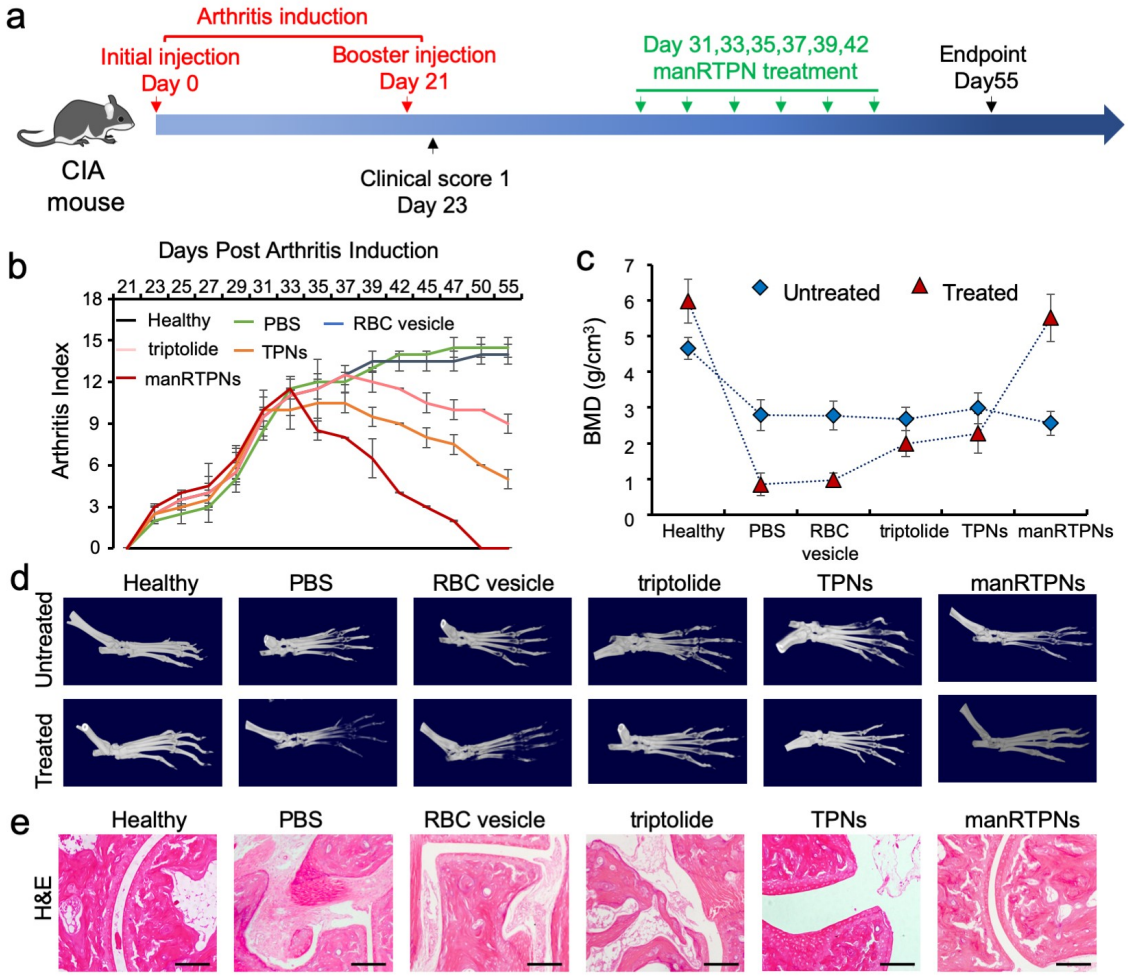

(a) The study protocol of a therapeutic regimen with CIA mice model. (b) Arthritis indexes of different treatment groups over 14 days; each experiment had five mice replicates. (c) Bone mean density (BMD) variation of the mice paw joints before and after different treatment. (d) Representative 3D reconstructed bone images of arthritic paws in different treatment groups.

(e) Representative images of H&E staining on knee sections from healthy mice and CIA mice treated with PBS, RBC vesicle, triptolide, TPNs or manRTPNs. Scale bars, 100 μm.

Figure 6. Shifting inflammatory factor of RA treatment by manRTPNs.

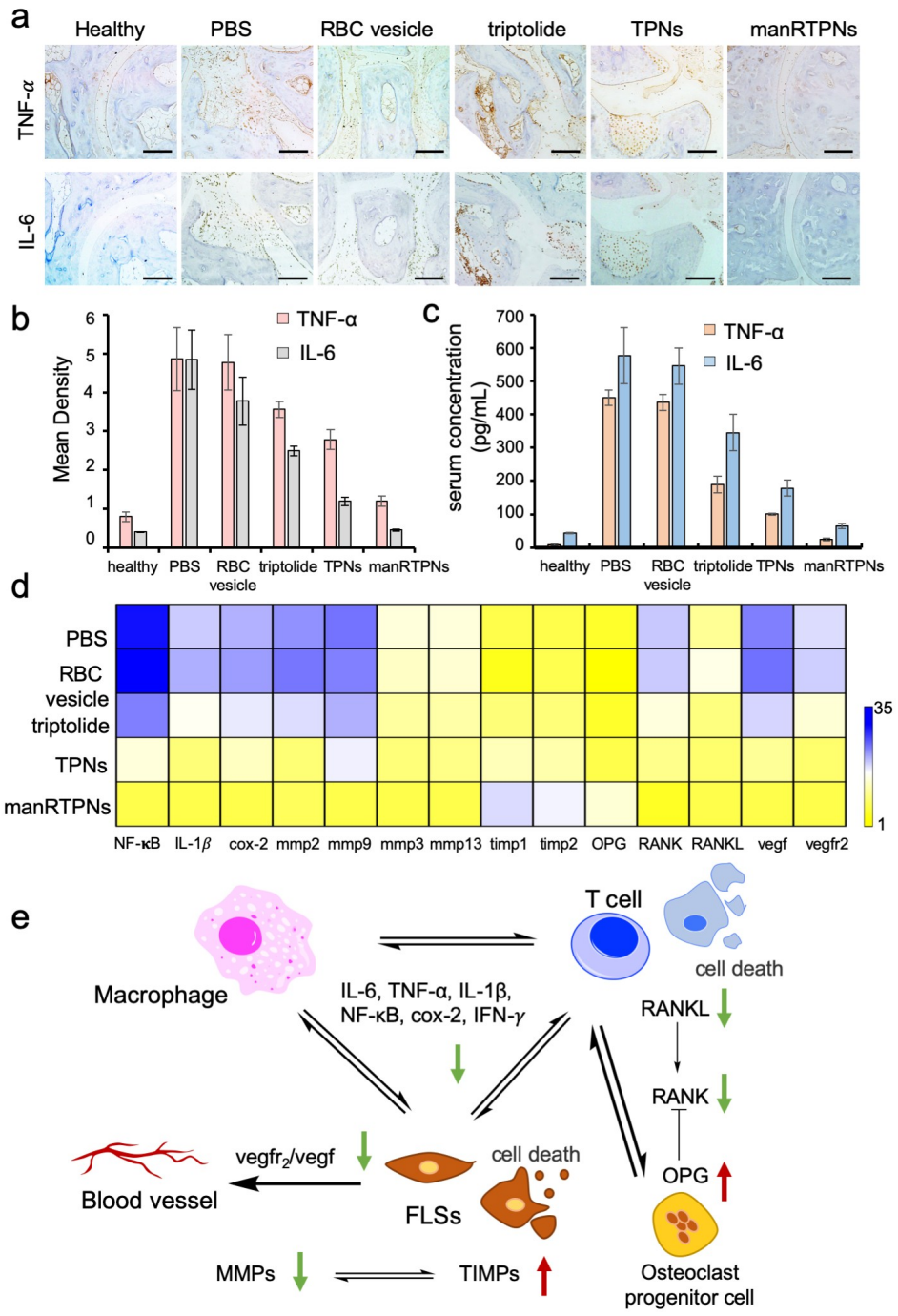

(a) Representative images of TNF-α and IL-6 immunohistochemical staining on knee sections. Scale bars, 100 μm. (b) Immunohistochemical quantification of TNF-α and IL-6. (c) Serum concentration of TNF-α and IL-6 in healthy mice and CIA mice treated with different groups. Each experiment point had three replicates. (d) Heatmap of genes expression profiles in different treatment. (e) Representative pathways alterations in manRTPNs remodeling RA inflammatory microenvironment.

Figure 7. Biocompatibility and safety of manRTPNs.

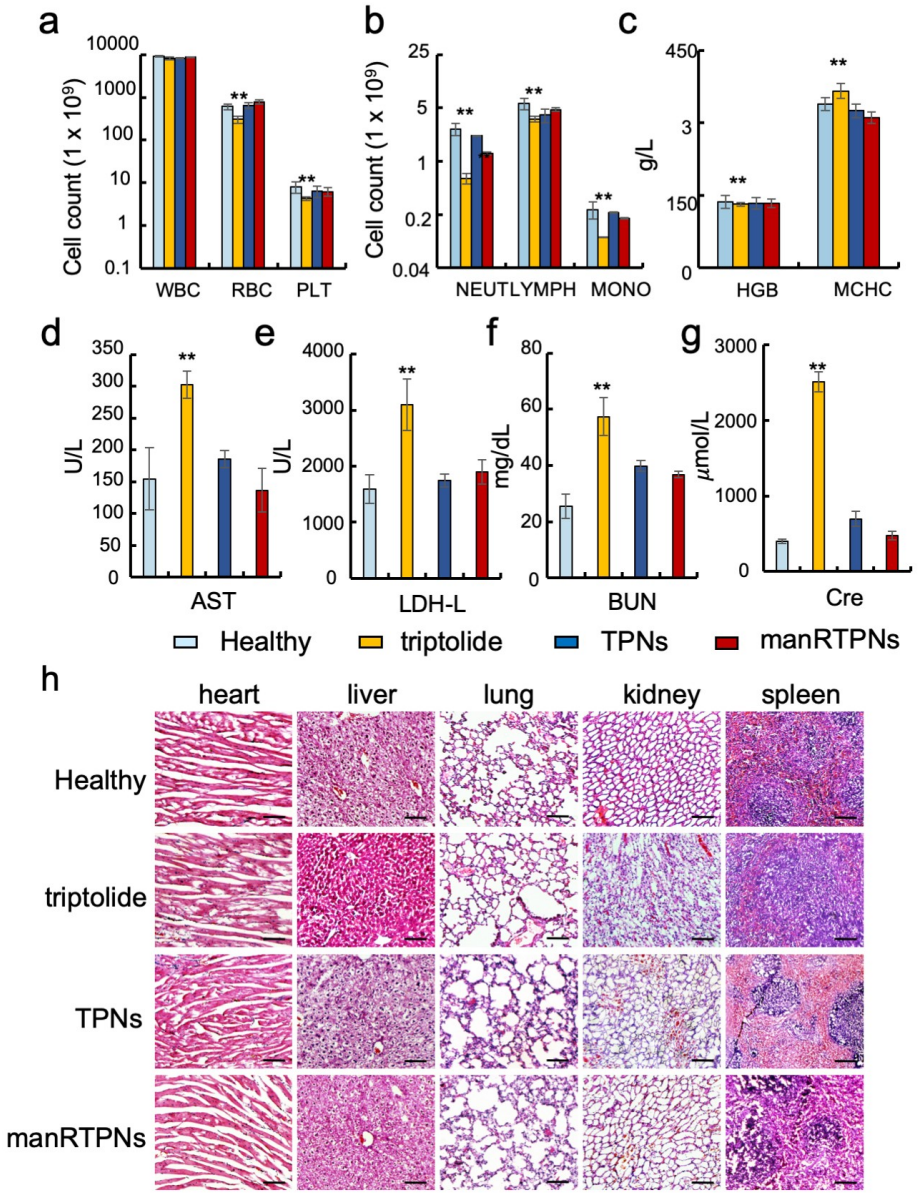

(a) Complete cell counts (white blood cells, red blood cells, and platelets) in PBS and triptolide-, TPNs-, manRTPNs-treated groups. Each experiment had three replicates. (b) Complete cell counts (neutrophil, lymphocyte, and monocyte) in PBS and triptolide-, TPNs-, manRTPNs-treated groups. Each experiment had three replicates. (c) Concentration of HGB and MCHC in four groups indicated before. Each experiment had three replicates. (d-g) Blood routine examination parameters including AST(d), LDH-L(e), BUN(f) and Cre(g) after

different treatment. Each experiment had three replicates. (h) H&E staining of main organs in four different groups. Scale bars, 100 μm.

SCHEME.

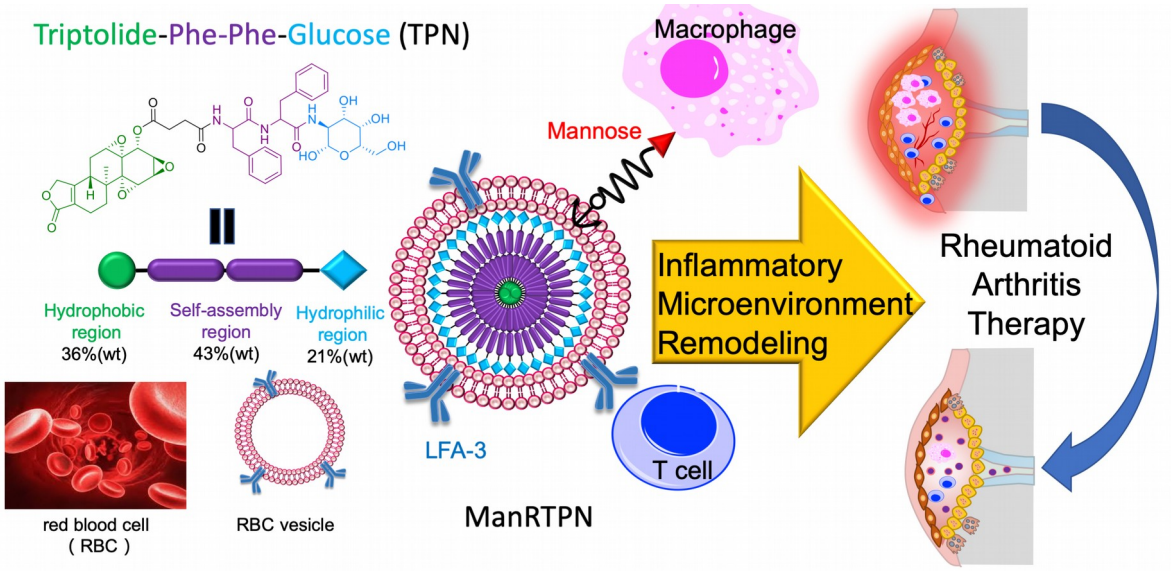

Schematic illustration of mannose modified erythrocyte membranes-coated triptolide nanoparticle (manRTPNs) targeting to inflammatory sites of rheumatoid arthritis and significant therapeutic effect. Targeting capacity to macrophages and T cells of manRTPNs is conferred from the mannose modified erythrocyte membrane. The binding is attributed to mannose and LFA-3 on the erythrocyte membranes, correspondingly CD206 overexpresses on activated macrophages and LFA-2 on T cells. TPNs at RA sites shift core genes expression in three pathways including angiogenesis, bone resorption and cytokine secretion.

Materials and Methods

Animal care

Mice were housed in an animal facility at Shenzhen Institutes of Advanced Technology, Chinese Academy of Sciences (SIAT). All animal experiments were performed in accordance with Guidance Suggestions for the Care and Use of Laboratory Animals and approved by Sciences Animal Care and Use Committee of SIAT.

Erythrocyte membranes derivation

Erythrocyte membranes were collected according to a previously reported method with modification. Briefly, fresh heparinized whole blood was collected from male mice (20-22 g) and subsequently centrifuged at 2000 rpm for 15 min at 4 °C to remove the plasma and the white buffy coat. The collected red blood cells were washed with 1× PBS three times and suspended in 0.25× PBS for 2 hours at 4 °C, and then the hemoglobin was removed by centrifugation at 9’000 rpm for 45 min. The resulting pink pellet was purified with 1× PBS, and the collected erythrocyte membrane was suspended and stored in distilled water. To form ligand-inserted erythrocyte ghosts, the light pink solution was incubated with DSPE-PEG-mannose for 30 min, 37°C water bath. Erythrocyte membranes with PEG-mannose or not was further prepared by extruding through a 200 nm polycarbonate porous membrane with an Avanti mini-extruder (Avanti Polar Lipids).

Synthesis of TPNs

The TPNs were synthesized by a prodrug self-assembly method. Briefly, after dissolving 5mmol Boc-Phe-Phe-OH (BOC-FF, J&K scientific Ltd., China), 6 mmol 1-Ethyl-3-(3-dimethylaminopropyl) carbodiimide (EDC, J&K scientific Ltd., China) and 6 mmol N-Hydroxysuccinimide (NHS, J&K scientific Ltd.,China) in 3 mL anhydrous DMF, another anhydrous DMF solution containing 5.5 mmol glucosamine (AG, Sigma-Aldrich, USA) and 5 mmol TEA (J&K scientific Ltd., China) was added drop-wise into it. The mixture was evaporated under reduced pressure for 24 hours to get crude product BOC-FF-AG. Then, crude BOC-FF-AG was dissolved in 30 mL equal volume mixture of anhydrous

dichloromethane and trifluoroacetic acid (TFA, J&K scientific Ltd., China) and stirred for 4 hours at room temperature. Afterward, pure NH_2-FF-AG was obtained after evaporated under reduced pressure and purified by silica gel column chromatography with dichloromethane and methanol. Secondly, 1 mmol triptolide (TP, Shanghai Yuanye Bio-Technology Co., Ltd., China), 1.2 mmol succinic anhydride (SAA, Sigma-Aldrich, USA) and 0.2 mmol dimethyl aminopyridine (DMAP, Sigma-Aldrich, USA) were dissolved in 3 mL pyridine and stirred overnight. After then, the mixture was diluted with ethyl acetate and washed it with solution containing saturated copper sulfate (J&K scientific Ltd.), water and brine. After reaction, residue TP-COOH was obtained through drying with anhydrous Na_2SO_4 and concentration with rotary evaporator. In the third step, TP-COOH, dicyclohexylcarbodiimide (DCC, Sigma-Aldrich, USA) and 1-hydroxy-5-pyrrolidinedione (NHS, J&K scientific Ltd., China) of equal molar ratio were dissolved into 3 mL anhydrous dichloromethane and stirred at room temperature for overnight. The final product TP-FF-AG was gained by reaction of activated TP-COOH and NH_2-FF-AG for overnight at room temperature and purified by analytical RP-HPLC and semi-preparative RP-HPLC with simultaneous detection at 265 nm. Analytical RP-HPLC was performed at room temperature on the Shimadzu LC 20 with UV detector SPD-20A using Inertsil ODS-SP column (4.6 x 250 mm, 5 μm, 100Å). The RP-HPLC gradient was started at 10% of B (CH_3CN, J&K scientific Ltd., China), then increased to 100% of B over 30 min (A: 0.1% TFA in water). Semi-preparative RP-HPLC was performed on the ULTIMAT 3000 Instrument (DIONEX). For fluorescence imaging experiments, Cyanine5.5 (Cy5.5, Lumiprobe, USA) was linked to intermediate product of NH_2-FF-AG

after esterification reaction to obtain Cy5.5-FF-AG in the same way. Ultimately, nanoparticles were self-assembled by added TP/Cy5.5-FF-AG dissolved in DMSO dropwise into PBS while vigorous stirring and dialysis for 2 days. ^{1}H NMR and ^{13}C NMR spectra were recorded with a Bruker VANCE III400 spectrometer (400 MHz). The high-resolution mass spectra (HR-MS) were measured on a Bruker Micro TOF II 10257 instrument. For membrane coating, nanoparticles were mixed with prepared membranes in ratio of 1:1. The resultant mixture was subsequently extruded nine times through a 200 nm polycarbonate porous membrane using an Avanti mini-extruder to yield the erythrocyte membranes-coating TPNs or mannose inserted erythrocyte membrane-coating TPNs (namely RTPNs or manRTPNs).

Nanoparticles Characterization

The hydrodynamic diameter and zeta potential of NPs suspended in 1 × PBS were measured by dynamic light scattering (DLS) (Zeta Plus, Brookhaven Instruments, USA). The morphologies of TPNs and manRTPNs were observed by transmission electron microscope (TEM, FEI spirit T12) at an accelerating voltage of 120 keV. The stability experiment of TPNs and manRTPNs in PBS was monitored by DLS over five weeks and stored at 4°C. The proteins retained on manRTPNs compared with those on the natural erythrocyte membrane were observed by SDS-PAGE. Briefly, 2mg of erythrocyte membrane vesicles and manRTPNs were collected by centrifugation at 15’000g for 30 min, mixed in SDS sample buffer (Invitrogen, USA), and heated at 90 °C for 5 min. Then, 20 μL of each sample was run on a 10% SDS-polyacrylamide gel (Bio-Rad, SDS-PAGE Gel Preparation Kit, USA) at 120 V for 1 h, followed by coomassie blue staining and imaging.

Pharmacokinetics

To evaluate the circulation half-life of TPNs and manRTPNs in vivo, 150 μL Cy5.5-labeled nanoparticles were injected into the tail vein of the mice (n = 3). Twenty microliters of blood were collected at 1, 5, 15, 30 min, and 1, 2, 4, 8, 24, 48, and 72 h following the injection. Each particle group contained 3-4 mice. The collected blood samples were diluted with 30 μL PBS in a 96-well plate before fluorescence measurement. Pharmacokinetics parameters were calculated to fit a two-compartment model and a one-way nonlinear model.

Drug toxicity analysis in vivo

Purchased from Vital River Laboratory Animal Technology Co. Ltd (Beijing, China), males BALB/c mice (6～8 weeks old) were randomly divided into four groups and intravenously injected with PBS, TPNs and manRTPNs at a single dosage of 25 mg/kg and triptolide of 15 mg/kg 4 times for eight days. A total of 7 days after last administration, all mice were euthanized, and blood was collected for and blood routine examination and biochemical parameters measurement, while main organs including heart, liver, spleen, lung, and kidney were excised and stained by H&E for histological analysis.

Cell culture

RAW264.7 cells, CTLL-2, RSC364 and hFLS-RA were purchased from the American Type Culture Collection (ATCC, USA) and cultured in Dulbecco's minimum essential medium (DMEM, Corning, USA) supplemented with 10% fetal bovine serum (FBS, Gibco, USA), 1% penicillin (100 IU/mL, Corning, USA), and streptomycin (100 μg/mL, Corning, USA)

and placed at 37 °C in a 5% CO2 humidified atmosphere. Cell lines were purchased with certification of authentication and free from Mycoplasma.

Quantification of cell targeting in vitro

A 6-well culture plate was prepared and RAW264.7, CTLL-2, RSC364 and hFLS-RA cells were implanted at a density of 5 × 105 cells/well. 12-16 hrs later, 80% of cell coverage was confirmed. 50 μL Cy5.5-labelled TPNs or manRTPNs was adding into prepared cells every hour for six hours, incubated with covering foil paper and collected them in the sixth hour. After digestion with trypsin (Gibco, USA), cells were put together and washed three times with ice-cold PBS, then underwent flow cytometry by FACS Canto II (BD Biosciences). The data was analyzed using Flow Jo software. Mean fluorescence intensity (MFI) reflected amount of intake nanoparticles amount. An uptake curve was constructed with MFI and time, and a k value being the slope of uptake curve was defined as uptake rate to measure targeting capacity of nanoparticles.

Immunofluorescence assay of macrophages and T cells with nanoparticles

Cells were cultured with medium added recombinant mouse IL-4 (100 ng/mL, R&D System, USA) or recombinant TNF-α (10 ng/mL, R&D System, USA) for six hours and incubated with TPNs, RTPNs or manRTPNs for 3 hours. Afterward, cells were fixed with 4% paraformaldehyde (Sigma-Aldrich, USA) for 10 minutes, permeabilized with 0.1% Triton™ X-100 (Sigma-Aldrich, USA) for 10 minutes, blocked with 1% BSA for 1 hour and labeled with 2 μg/mL anti-mannose receptor/AF488 conjugated antibody (ab195191, Abcam) and rabbit anti-LFA-2/AF488 conjugated antibody (bs-2899R, Bioss) for 3 hours at room

temperature. Nuclei were stained with DAPI. All manipulation must be away from light. The images were captured under confocal microscopy (Leica, TCS SP5).

Cytotoxicity Study in vitro

The cellular toxicities of TPNs and manRTPNs on macrophages, T cells, FLSs and hFLSs were determined by MTT assay using CCK-8 Kit. Cells were implanted in a 96-well culture plate at a density of 8 × 103 cells/well (5 replicates each treated group). After 12 hrs, PBS, TPNs and manRTPNs with concentrations of 10 nM, 50 nM, 100 nM, 200 nM, 500 nM were added into medium for further 24 hrs co-culture. Then the cells were mildly washed by PBS before added CCK-8 mixed solution. Then, the optical density in 450 nm was measured by Multiskan GO (Thermo Fisher Scientific).

Cytokines concentration analysis

The TNF-α, IL-6 and IFN-γ concentrations of cells culture supernatants were determined with ELISA Kit using mouse ELISA Kits (Biolegend, USA) as manipulation. Also, the TNF-α and IL-6 concentrations of mouse serum samples were determined with TNF-α and IL-6 ELISA Kits (Biolegend, USA). Briefly, Serum samples of treated mice were collected at the end of experiment and concentrations of TNF-α and IL-6 were quantified with ELISA kits. Specifically, the whole blood of mice was collected by submandibular bleeding into microtubes and allowed to clot at room temperature for 30 min. Samples were then centrifuged at 2,000g for 6 min to collect supernatant serum. Serum samples were immediately frozen at -20 °C until analysis by using mouse TNF-α and mouse IL-6 ELISA kits (Biolegend) within 3 days of collection.

Genes expression profiles analysis of cells

After treated with nanoparticles of serious concentrations, cells were harvested to isolate RNA. RNA was extracted with TRIzol reagent (Invitrogen, USA) according to the manufacturer's instructions. Complementary DNAs (cDNAs) were synthesized with QuantiTect Reverse Transcription Kit (QIAGEN K.K., Tokyo, Japan) and the specific gene transcripts were quantified by quantitative real-time PCR using QuantiTect SYBR Green PCR Kit (QIAGEN K.K., Tokyo, Japan) and analyzed with ABI 7500 real-time PCR system (Applied Biosystems, USA). The gene expression patterns along with concentration were highlight with heatmap by using TBtools package.

Collagen induced arthritis (CIA) mice model induction

Seventy-two female DBA/1 mice (6～8 weeks old) were purchased from Vital River Laboratory Animal Technology Co. Ltd (Beijing, China). All mice were maintained in a SF system which is room equipped with an air-filtering system, and the cages and water were sterilized. CIA was induced as previously reported study [38]. Briefly, bovine type II collagen (Chondrex, Redmond, WA, USA) was dissolved in 0.1M acetic acid overnight at 4°C. This was emulsified in an equal volume of complete Freund's adjuvant (Chondrex, Redmond, WA, USA). The mice were immunized intradermal at the base of the tail with 100 μL of emulsion containing 100 μg of type II collagen. On day 21, mice were boosted intraperitoneal with 100 μg type II collagen dissolved in phosphate buffered saline (PBS). Clinical scores of each hindpaws and forepaws of mice were obtained following the standard evaluation process [38]. In detail, no evidence of erythema and swelling occurred is score 0, erythema and mild

swelling appeared is score 1, erythema and mild swelling extended from the ankle to the tarsals is score 2, erythema and moderate swelling extended from the ankle to metatarsal joints is score 3 and erythema and severe swelling encompassed the ankle, paws, and digits or ankyloses of the limb is score 4. Then total clinical scores of hindpaws and forepaws were calculated. At least six mice each group.

Inflamed joints imaging in vivo

After CIA model was established, free Cy5.5, Cy5.5-labelled TPNs and manRTPNs were intravenously injected into the CIA mice (20 mg/kg, n = 4). Fluorescence images were obtained after 1, 2, 4, 8, 12, and 24 hours using an in vivo imaging system (IVIS, Caliper, USA). Then, the mice were sacrificed for ex vivo tissue/organs distribution analysis at the end of experiment. Meanwhile, the synovial tissue was dissected and dehydrated in 30% sucrose solution overnight and then cry-sectioned at 8 μm. The sections were stained with DAPI and washed twice. Fluorescence images were obtained using a confocal microscope (Leica, TCS SP5). The fluorescence intensity of sections in different groups was calculated using software Image J.

In vivo efficacy of manRTPNs

According to CIA mice model conduction, starting at day 21, the clinical scores were calculated to make sure that CIA mice were almost equably and randomly divided into four groups, while healthy DBA/1 mice were set as control (n = 5). Five different agents namely PBS, RBC vesicle, triptolide, TPNs and manRTPNs were intravenously injected every two days. The timeline of whole therapy experiment from model making to the end was according

to schematic diagram shown in **figure** 5A. The arthritis index of each group was recorded over time to evaluate treatment efficacy. At the end, the mice were sacrificed for further analysis.

Micro-CT imaging of mice paws

The knee and ankle joints of each experimental mouse hindpaws were scanned using micro-CT system (Bruker's SkyScan 1278, UK) to observe joint bone situation. Images were acquired at 55 kV, 72 μA and 300 ms/frame, with 360 views. The 3D structures of knee joint and ankle joint were reconstructed from 360 views and BDM was evaluated by corresponding SkyScan NRecon package. Analysis typically took around 15 min per joint for an experienced operator.

Histological analysis

At study endpoints, mice were euthanized and hind knee joints were collected for H&E staining and immunohistochemical staining. Briefly, the ankle and knee joints of scarified animals as well as their heart, liver, spleen, lung and kidney were fixed in 10% buffered formalin and then joints were incubated in decalcifying solution (4% hydrochloric acid in 4% formaldehyde) at room temperature for 7 days for decalcification. After paraffinization, microtome (Leica) slices of 8 μm were prepared and stained with haematoxylin and eosin, images were taken by using inverted microscope (Olympus, IX71, Japan) and the inflammatory cell infiltration in synovial tissues, bone and cartilage was evaluated by Image J software.

Immunohistochemical staining assay

After deparaffinization the slices were subjected to antigen recovery in 0.01 M sodium citrate buffer at 125 °C for 30 s, followed by 10 s at 90 °C, and then subjected to the endogenous peroxidase inactivation by covering tissue with 3% hydrogen peroxide for 5 min. After blocking non-specific binding sites with 10% goat serum in PBS, the slices were incubated with TNF-α / IL-6 monoclonal antibody (Invitrogen) with a dilution rate of 1:100, respectively, at 4 °C for 24 h. Then the slices were incubated with horseradish peroxidase (HRP)-conjugated secondary antibody with a dilution rate of 1:800 at 37 °C for 1 h. Sections were developed using the DAB substrate and then counterstained with haematoxylin. The images were captured and analyzed by inverted microscope (Olympus, IX71, Japan) and Image J software.

Gene expression profiles analysis of tissues

The paws and ankles were dissected from mice on day 22 of arthritis, snap-frozen in liquid nitrogen, ground into powder, and homogenized. All procedure must be under RNase-free conditions. The RNA isolation and real-time PCR assay were carried out following the protocol following. Briefly, total RNA was extracted with TRIzol reagent (Invitrogen, Carlsbad, CA, USA) from the tissue homogenates according to the manufacturer's instructions. The total RNA (1 μg) was reverse transcribed to cDNA using the QuantiTect Reverse Transcription Kit (QIAGEN, Japan) and the specific gene transcripts were quantified by quantitative real-time PCR using QuantiTect SYBR Green PCR Kit (QIAGEN K.K., Tokyo, Japan) and analyzed with ABI 7500 real-time PCR system (Applied Biosystems, USA). PCR was performed as 40 cycles at 94°C for 15 s, 55°C for 30 s, and 72°C for 30 s.

The relative RNA expression was calculated with comparative *CT* method; β-actin as internal control. The gene expression patterns along with concentration were highlight with heatmap by using TBtools package. Gene-specific primers were synthesized by Sangon Biotech (Shanghai) Co., Ltd. and list in the table.

ASSOCIATED CONTENT

Supporting Information. A listing of the contents of each file supplied as Supporting Information should be included. Table. Gene-specific primers were listed. Triptolide prodrug synthesis process; ^{1}H NMR spectrum and ^{13}C NMR spectrum of TP-COOH ; ^{1}H NMR spectrum and ^{13}C NMR spectrum of BOC-FF-AG; ^{1}H NMR spectrum and ^{13}C NMR spectrum of NH_2-FF-AG; ^{1}H NMR spectrum and ^{13}C NMR spectrum of TP-FF-AG; ^{1}H NMR spectrum and ^{13}C NMR spectrum of Cy5.5-FF-AG; HPLC calibration curve for monomer (HPMA) with UV/Vis absorbance at 254 nm; MS of BOC-FF-AG, TP-COOH; Cy5.5-FF-AG; NH_2-FF-AG and TP-FF-AG; Protein composition of RBC vesicles and manRTPNs analyzed by SDS-PAGE; FACS analysis of untreated and treated RAW264.7 in 6 hrs; FACS analysis of untreated and treated CTLL-2 in 6 hrs; FACS analysis of untreated and trated RSC364 in 6 hrs; Cellular uptake and cytotoxicity of manRTPNs in hFLS-RA; FACS analysis of hFLS in 6 hrs; A clinical scoring of swelling degree and micro-CT of bone erosion in CIA mice model; The survival rate of mice administered with different triptolide formulations. (file type, PDF)

AUTHOR INFORMATION

Corresponding Author

*(Pf. Z.) E-mail addresses: pf.zhang@siat.ac.cn.

*(P. G.) E-mail addresses: ping.gong@siat.ac.cn.

*(Lt. C.) E-mail addresses: lt.cai@siat.ac.cn.

Author Contributions

J.L., P.G. and L.T.C. conceived and designed the work. J.L. and S.P.L. performed all experiments. C.B.L and H.F.L helped with experiments. C.J.L participated in the work. All authors analyzed and discussed the data. J.L., P.F.Z and L.T.C. wrote the manuscript.

ACKNOWLEDGMENT

This work was supported by National Natural Science Foundation of China (81801838, 31571013, 81701816 and 81601552), Guangdong Natural Science Foundation of Research Team (2016A030312006), K.C. Wong Education Foundation (GJTD-2018-14), Natural Science Foundation of Guangdong Province (2018A030313013), Shenzhen Science and Technology Program (JCYJ20180302145912832, JCYJ20160429191503002, JCYJ20170818162259843 and JCYJ20170818163739458). Importantly, thanks to professor Hong Chang Li and Dr. Yi Fan Ma for their useful and meaningful recommendations to improve this paper.

REFERENCES

1. Scott, D. L.; Wolfe, F.; Huizinga, T. W. J., Rheumatoid Arthritis. *Lancet* **2010,** *376* (9746), 1094-1108.

2. Pincus, T.; Brooks, R. H.; Callahan, L. F., Prediction of Long-Term Mortality in Patients with Rheumatoid-Arthritis According to Simple Questionnaire and Joint Count Measures. *Annals of Internal Medicine* **1994,** *120* (1), 26-34.

3. van Vollenhoven, R. F., Treatment of Rheumatoid Arthritis: State of the Art 2009. *Nat Rev Rheumatol* **2009,** *5* (10), 531-541.

4. Bykerk, V., Unmet Needs in Rheumatoid Arthritis. *J Rheumatol* **2009,** *36*, 42-46.

5. Salliot, C.; van der Heijde, D., Long-term Safety of Methotrexate Monotherapy in Patients with Rheumatoid Arthritis: A Systematic Literature Research. *Ann Rheum Dis* **2009,** *68* (7), 1100-1104.

6. Alcorn, N.; Saunders, S.; Madhok, R., Benefit-Risk Assessment of Leflunomide An Appraisal of Leflunomide in Rheumatoid Arthritis 10 Years After Licensing. *Drug Safety* **2009,** *32* (12), 1123-1134.

7. Leombruno, J. P.; Einarson, T. R.; Keystone, E. C., The Safety of Anti-tumour Necrosis Factor Treatments in Rheumatoid Arthritis: Meta and Exposure-adjusted Pooled Analyses of Serious Adverse Events. *Ann Rheum Dis* **2009,** *68* (7), 1136-1145.

8. Hyrich, K. L.; Watson, K. D.; Isenberg, D. A.; Symmons, D. P. M.; Register, B. B., The British Society for Rheumatology Biologics Register: 6 Years on. *Rheumatology* **2008,** *47* (10), 1441-1443.

9. Kirwan, J. R.; Bijlsma, J. W. J.; Boers, M.; Shea, B. J., Effects of Glucocorticoids on Radiological Progression in Rheumatoid Arthritis. *Cochrane Db Syst Rev* **2007,** *2007* (1), CD006356.

10. Ravindran, V.; Rachapalli, S.; Choy, E. H., Safety of Medium- to Long-term Glucocorticoid Therapy in Rheumatoid Arthritis: A Meta-Analysis. *Rheumatology* **2009,** *48* (7), 807-811.

11. Elshabrawy, H. A.; Chen, Z. L.; Volin, M. V.; Ravella, S.; Virupannavar, S.; Shahrara, S., The Pathogenic Role of Angiogenesis in Rheumatoid Arthritis. *Angiogenesis* **2015,** *18* (4), 433-448.

12. Zhang, Q. Z.; Dehaini, D.; Zhang, Y.; Zhou, J. L.; Chen, X. Y.; Zhang, L. F.; Fang, R. H.; Gao, W. W.; Zhang, L. F., Neutrophil Membrane-coated Nanoparticles Inhibit Synovial Inflammation and Alleviate Joint Damage in Inflammatory Arthritis. *Nat Nanotechnol* **2018,** *13* (12), 1182-1190.

13. Li, R. X.; He, Y. W.; Zhu, Y.; Jiang, L. X.; Zhang, S. Y.; Qin, J.; Wu, Q.; Dai, W. T.; Shen, S.; Pang, Z. Q.; Wang, J. X., Route to Rheumatoid Arthritis by Macrophage-derived Microvesicle-coated Nanoparticles. *Nano Letters* **2019,** *19* (1), 124-134.

14. Liang, H. Y.; Peng, B.; Dong, C.; Liu, L. X.; Mao, J. J.; Wei, S.; Wang, X. L.; Xu, H. S.; Shen, J.; Mao, H. Q.; Gao, X. H.; Leong, K. W.; Chen, Y. M., Cationic Nanoparticle as An Inhibitor of Cell-free DNA-induced Inflammation. *Nat Commun* **2018,** *9*, 4291.

15. Liu L., H. F., Wang H., Wu X., Eltahan A.S., Stanford S., Bottini N., Xiao H., Bottini M., Guo W., Liang X.J., Secreted Protein Acidic and Rich in Cysteine Mediated Biomimetic Delivery of Methotrexate by Albumin-Based Nanomedicines for Rheumatoid Arthritis Therapy. *ACS Nano.* **2019,** *13* (5), 5036-5048.

16. Tao X; Cush JJ; Garret M; PE., L., A Phase I Study Of Ethylacetate Extract of the Chinese Antirheumatic Herb *Tripterygium wilfordii Hook F* in Rheumatoid Arthritis. *J. Rheumatol* **2001,** *28*, 2167.

17. Fan, D. P.; Guo, Q. Q.; Shen, J. W.; Zheng, K.; Lu, C.; Zhang, G.; Lu, A. P.; He, X. J., The Effect of Triptolide in Rheumatoid Arthritis: From Basic Research towards Clinical Translation. *Int J Mol Sci.* **2018,** *19* (2), 376.

18. Yuan, Z. X.; Wu, X. J.; Mo, J. X.; Wang, Y. L.; Xu, C. Q.; Lim, L. Y., Renal Targeted Delivery of Triptolide by Conjugation to the Fragment Peptide of Human Serum Albumin. *Eur J Pharm Biopharm* **2015,** *94*, 363-371.

19. Pao, H. P.; Liao, W. I.; Wu, S. Y.; Hung, K. Y.; Huang, K. L.; Chu, S. J., PG490-88, A Derivative of Triptolide, Suppresses Ischemia/Reperfusion-Induced Lung Damage By Maintaining Tight Junction Barriers and Targeting Multiple Signaling Pathways. *International Immunopharmacology* **2019,** *68*, 17-29.

20. He, Q. L.; Minn, I.; Wang, Q. L.; Xu, P.; Head, S. A.; Datan, E.; Yu, B.; Pomper, M. G.; Liu, J. O., Targeted Delivery and Sustained Antitumor Activity of Triptolide through Glucose Conjugation. *Angew Chem Int Edit* **2016,** *55* (39), 12035-12039.

21. He J, P. T., Peng Y, Ai L, Deng Z, Wang XQ, Tan W, Molecularly Engineering Triptolide with Aptamers for High Specificity and Cytotoxicity for Triple-Negative Breast Cancer. *J Am Chem Soc*. **2020,** *142* (6), 2699-2703.

22. Huang, C. L.; Zeng, T.; Li, J. W.; Tan, L. S.; Deng, X. L.; Pan, Y. C.; Chen, Q.; Li, A. Q.; Hu, J. Q., Folate Receptor-Mediated Renal-Targeting Nanoplatform for the Specific Delivery of Triptolide to Treat Renal Ischemia/Reperfusion Injury. *Acs Biomater Sci Eng* **2019,** *5* (6), 2877-2886.

23. Ling, D.; Xia, H.; Park, W.; Hackett, M. J.; Song, C.; Na, K.; Hui, K. M.; Hyeon, T., pH-Sensitive Nanoformulated Triptolide as a Targeted Therapeutic Strategy for Hepatocellular Carcinoma. *Acs Nano* **2014,** *8* (8), 8027-8039.

24. Brannon-Peppas L, B. J., Nanoparticle and Targeted Systems for Cancer Therapy. *Adv Drug Deliv Rev.* **2004,** *56* (11), 1649-1659.

25. Abbas, M.; Zou, Q. L.; Li, S. K.; Yan, X. H., Self-Assembled Peptide- and Protein-Based Nanomaterials for Antitumor Photodynamic and Photothermal Therapy. *Advanced Materials* **2017,** *29* (12).

26. Zhu, P. L.; Yan, X. H.; Su, Y.; Yang, Y.; Li, J. B., Solvent-Induced Structural Transition of Self-Assembled Dipeptide: From Organogels to Microcrystals. *Chem-Eur J* **2010,** *16* (10), 3176-3183.

27. Yan, X. H.; Zhu, P. L.; Li, J. B., Self-assembly and Application of Diphenylalanine-based Nanostructures. *Chem Soc Rev* **2010,** *39* (6), 1877-1890.

28. Du W, H. X., Wei W, Liang G., Intracellular Peptide Self-Assembly: A Biomimetic Approach for in Situ Nanodrug Preparation. *Bioconjug Chem.* **2018,** *29* (4), 826-837.

29. Kinne, R. W.; Brauer, R.; Stuhlmuller, B.; Palombo-Kinne, E.; Burmester, G. R., Macrophages in Rheumatoid Arthritis. *Arthritis Res* **2000,** *2* (3), 189-202.

30. Udalova IA, M. A., Feldmann M., Macrophage Heterogeneity in the Context of Rheumatoid Arthritis. *Nat Rev Rheumatol.* **2016,** *12* (8), 472-485.

31. Toh ML, M. P., The Role of T Cells in Rheumatoid Arthritis: New Subsets and New Targets. *Curr Opin Rheumatol.* **2007,** *19* (3), 284-288.

32. Mellado M, M.-M. L., Cascio G, Lucas P, Pablos JL, Rodríguez-Frade JM., T Cell Migration in Rheumatoid Arthritis. . *Front Immunol.* **2015,** *6*, 384.

33. Niedermeier M, P. T., Korb A., Therapeutic Opportunities in Fibroblasts in Inflammatory Arthritis. *Best Pract Res Clin Rheumatol.* **2010,** *24* (4), 527-540.

34. Put S, W. R., Lahoutte T, Matthys P., Molecular Imaging of Rheumatoid Arthritis: Emerging Markers, Tools, and Techniques. *Arthritis Res Ther.* **2014,** *16* (2), 208.

35. Davis, S. J.; Ikemizu, S.; Evans, E. J.; Fugger, L.; Bakker, T. R.; van der Merwe, P. A., The Nature of Molecular Recognition by T cells. *Nat Immunol* **2003,** *4* (3), 217-224.

36. Raychaudhuri, S.; Thomson, B. P.; Remmers, E. F.; Eyre, S.; Hinks, A.; Guiducci, C.; Catanese, J. J.; Xie, G.; Stahl, E. A.; Chen, R.; Alfredsson, L.; Amos, C. I.; Ardlie, K. G.; Barton, A.; Bowes, J.; Burtt, N. P.; Chang, M.; Coblyn, J.; Costenbader, K. H.; Criswell, L.

A.; Crusius, J. B. A.; Cui, J.; De Jager, P. L.; Ding, B.; Emery, P.; Flynn, E.; Harrison, P.; Hocking, L. J.; Huizinga, T. W. J.; Kastner, D. L.; Ke, X. Y.; Kurreeman, F. A. S.; Lee, A. T.; Liu, X. D.; Li, Y. H.; Martin, P.; Morgan, A. W.; Padyukov, L.; Reid, D. M.; Seielstad, M.; Seldin, M. F.; Shadick, N. A.; Steer, S.; Tak, P. P.; Thomson, W.; van der Helm-van Mil, A. H. M.; van der Horst-Bruinsma, I. E.; Weinblatt, M. E.; Wilson, A. G.; Wolbink, G. J.; Wordsworth, P.; Altshuler, D.; Karlson, E. W.; Toes, R. E. M.; de Vries, N.; Begovich, A. B.; Siminovitch, K. A.; Worthington, J.; Klareskog, L.; Gregersen, P. K.; Daly, M. J.; Plenge, R. M.; Consortium, B.; Consortium, Y., Genetic Variants at CD28, PRDM1 and CD2/CD58 are Associated with rheumatoid Arthritis Risk. *Nat Genet* **2009,** *41* (12), 1313-1318.

37. Sable, R.; Durek, T.; Taneja, V.; Craik, D. J.; Pallerla, S.; Gauthier, T.; Jois, S., Constrained Cyclic Peptides as Immunomodulatory Inhibitors of the CD2:CD58 Protein-Protein Interaction. *Acs Chemical Biology* **2016,** *11* (8), 2366-2374.

38. Rossi, L.; Fraternale, A.; Bianchi, M.; Magnani, M., Red Blood Cell Membrane Processing for Biomedical Applications. *Frontiers in Physiology* **2019,** *10*.

39. Hu, C. M. J.; Fang, R. H.; Copp, J.; Luk, B. T.; Zhang, L. F., A Biomimetic Nanosponge that Absorbs Pore-forming Toxins. *Nat Nanotechnol* **2013,** *8* (5), 336-340.

40. He, Q. L.; Titov, D. V.; Li, J.; Tan, M. J.; Ye, Z. H.; Zhao, Y. M.; Romo, D.; Liu, J. O., Covalent Modification of a Cysteine Residue in the XPB Subunit of the General Transcription Factor TFIIH Through Single Epoxide Cleavage of the Transcription Inhibitor Triptolide. *Angew Chem Int Edit* **2015,** *54* (6), 1859-1863.

41. Fang, R. N. H.; Hu, C. M. J.; Chen, K. N. H.; Luk, B. T.; Carpenter, C. W.; Gao, W. W.; Li, S. L.; Zhang, D. E.; Lu, W. Y.; Zhang, L. F., Lipid-insertion Enables Targeting Functionalization of Erythrocyte Membrane-cloaked Nanoparticles. *Nanoscale* **2013,** *5* (19), 8884-8888.

42. Shao, F.; Wang, G. J.; Xie, H. T.; Zhu, X. Y.; Sun, J. G.; A, J. Y., Pharmacokinetic Study of Triptolide, a Constituent of Immunosuppressive Chinese Herb Medicine, in Rats. *Biological & Pharmaceutical Bulletin* **2007,** *30* (4), 702-707.

43. Ghosh, S.; Hayden, M. S., New Regulators of NF-kappaB in Inflammation. *Nat Rev Immunol* **2008,** *8* (11), 837-848.

44. Brand, D. D.; Latham, K. A.; Rosloniec, E. F., Collagen-induced Arthritis. *Nat Protoc* **2007,** *2* (5), 1269-1275.

45. Noack, M.; Miossec, P., Selected Cytokine Pathways in Rheumatoid Arthritis. *Semin Immunopathol* **2017,** *39* (4), 365-383.

46. Geusens, P., The Role of RANK Ligand/osteoprotegerin in Rheumatoid Arthritis. *Ther Adv Musculoskelet Dis* **2012,** *4* (4), 225-233.